ISSN 2176-5480

22nd International Congress of Mechanical Engineering (COBEM 2013)
November 3-7, 2013, Ribeirão Preto, SP, Brazil

ON THE FINITE ELEMENT CHARACTERIZATION OF d_{31} MACRO-FIBRE COMPOSITES EFFECTIVE PROPERTIES

Marcelo A. Trindade
São Carlos School of Engineering, University of São Paulo, 13566-590 São Carlos, Brazil
trindade@sc.usp.br

Ayech Benjeddou
Institut Supérieur de Mécanique de Paris, Structures, 93407 Saint Ouen CEDEX, France
benjeddou@supmeca.fr

Abstract. *This work presents the characterization of effective properties of a d_{31} piezoelectric Macro-Fibre Composite (MFC) using a finite element homogenization technique, accounting in particular for the effect of electrode and protective layers on the effective elastic, piezoelectric and dielectric coefficients. Then, an analysis of the effect of the fibre volume fraction and electric boundary conditions on the main effective properties is presented. Results indicate that the effective properties may be substantially reduced by the protective and electrode layers and, thus, they must be accounted for in order to obtain a proper predictive model.*

Keywords: *Macro-Fibre Composites, Finite Element Homogenization, Properties Characterization, Mixture Rules.*

1. INTRODUCTION

Piezoelectric Macro-Fibre Composites (MFC) are widely used as distributed sensors for several applications such as structural health monitoring and energy harvesting since they combine conformability and high sensitiveness to mechanical strains (Wilkie et al., 2000). Nowadays, they can be found commercially in the two operation modes, so-called d_{33} and d_{31} (Smart Material Co., 2009). Alternative designs using the d_{15} operation modes have been proposed (Gajewski, 2011; Raja and Ikeda, 2008; Trindade and Benjeddou, 2011, 2013) but are not yet commercially available. As actuators, they are mostly used as 'free or displacement actuators' for applications such as pumps and valves. This is because their performance as 'force actuators' is limited by the loss of transmissibility between the MFC and the host structure caused by the MFC packaging. The performance of an MFC as strain sensors is normally related to its strain piezoelectric coefficient d_{ij}, while its performance as force actuators depends on its stress piezoelectric coefficient e_{ij}.

Since MFC transducers are heterogeneous and made of several different materials (piezoceramic fibres, epoxy matrix, electrode layers and protective layers), a methodology is required to relate the piezoceramic fibres material properties to the effective MFC ones and, thus, estimate the effective piezoelectric coefficients d_{ij} and e_{ij}. Substantial research effort has been directed to the characterization of their effective material properties, as in (Deraemaeker et al., 2009; Deraemaeker and Nasser, 2010) for d_{31} and d_{33} MFCs and (Benjeddou and Al-Ajmi, 2009; Kranz, Benjeddou and Drossel, 2013; Trindade and Benjeddou, 2011, 2013) for d_{15} MFCs. Some of these studies (Gajewski, 2011; Kranz, Benjeddou and Drossel, 2013; Trindade and Benjeddou, 2011) have shown that the effective properties depend not only on the piezoceramic fibres, epoxy materials and fibre volume fraction of the active layer but also on the geometrical and material properties of the protective and electrode layers. Indeed, analytical and numerical homogenization techniques have been proposed for the active layer only (Deraemaeker et al., 2009; Benjeddou and Al-Ajmi, 2009) but they fail to capture the effect of the electrode and protective layers which seems to be particularly important for 'force actuators' applications.

This work presents the characterization of effective properties of a d_{31} piezoelectric MFC using a finite element homogenization technique, accounting in particular for the effect of electrode and protective layers on the effective elastic, piezoelectric and dielectric coefficients. Then, an analysis of the effect of the fibre volume fraction and electric boundary conditions on the main effective properties is presented.

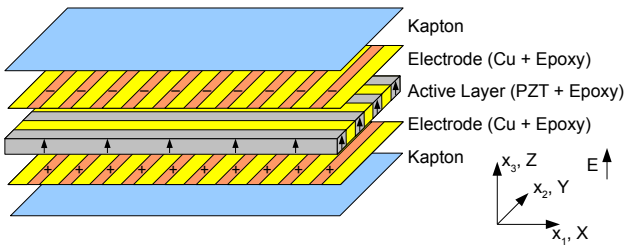

Figure 1. Schematic representation of a d_{31} Macro-Fibre Composite.

ISSN 2176-5480

2. ASSUMED CONSTITUTIVE EQUATIONS FOR d_{31} MFC

The d_{31} MFC considered is made of an active layer, composed of piezoceramic macro-fibres embedded in an Epoxy matrix. The active layer is then covered by electrode and protective layers, as shown in Figure 1. The piezoelectric material is considered to be poled in x_3 direction with electrodes fully covering top (x_3^+) and bottom (x_3^-) surfaces such that a preferential or dominant x_3 direction is imposed for the electric field and displacement. Therefore, it can be assumed that $E_1 = E_2 = 0$ and the following reduced constitutive equations can be written

$$\left\{\begin{array}{c} T_1 \\ T_2 \\ T_3 \\ T_4 \\ T_5 \\ T_6 \\ \hline D_3 \end{array}\right\} = \left[\begin{array}{cccccc|c} c_{11}^E & c_{12}^E & c_{13}^E & 0 & 0 & 0 & -e_{31} \\ c_{12}^E & c_{22}^E & c_{23}^E & 0 & 0 & 0 & -e_{32} \\ c_{13}^E & c_{23}^E & c_{33}^E & 0 & 0 & 0 & -e_{33} \\ 0 & 0 & 0 & c_{44}^E & 0 & 0 & 0 \\ 0 & 0 & 0 & 0 & c_{55}^E & 0 & 0 \\ 0 & 0 & 0 & 0 & 0 & c_{66}^E & 0 \\ \hline e_{31} & e_{32} & e_{33} & 0 & 0 & 0 & \epsilon_{33}^S \end{array}\right] \left\{\begin{array}{c} S_1 \\ S_2 \\ S_3 \\ S_4 \\ S_5 \\ S_6 \\ \hline E_3 \end{array}\right\}, \tag{1}$$

$$\left\{\begin{array}{c} S_1 \\ S_2 \\ S_3 \\ S_4 \\ S_5 \\ S_6 \\ \hline D_3 \end{array}\right\} = \left[\begin{array}{cccccc|c} s_{11}^E & s_{12}^E & s_{13}^E & 0 & 0 & 0 & d_{31} \\ s_{12}^E & s_{22}^E & s_{23}^E & 0 & 0 & 0 & d_{32} \\ s_{13}^E & s_{23}^E & s_{33}^E & 0 & 0 & 0 & d_{33} \\ 0 & 0 & 0 & s_{44}^E & 0 & 0 & 0 \\ 0 & 0 & 0 & 0 & s_{55}^E & 0 & 0 \\ 0 & 0 & 0 & 0 & 0 & s_{66}^E & 0 \\ \hline d_{31} & d_{32} & d_{33} & 0 & 0 & 0 & \epsilon_{33}^T \end{array}\right] \left\{\begin{array}{c} T_1 \\ T_2 \\ T_3 \\ T_4 \\ T_5 \\ T_6 \\ \hline E_3 \end{array}\right\}, \tag{2}$$

where T_p and S_q, with $p,q = 1,\ldots,6$, denote the six components of mechanical stress and strain vectors in Voigt notation. D_3 and E_3 denote the transverse electric displacement and field. For the e-form, c_{pq}^E, e_{3j} $(j = 1,2,3)$ and ϵ_{33}^S denote the elastic stiffness (at constant electric fields), piezoelectric and electric permittivity (at constant mechanical strains) coefficients. For the d-form, s_{pq}^E, d_{3j} $(j = 1,2,3)$ and ϵ_{33}^T denote the elastic compliance (at constant electric fields), piezoelectric and electric permittivity (at constant mechanical stresses) coefficients.

It is also worthwhile considering reduced constitutive equations using a plane-stress state $T_3 = 0$. The plane-stress assumption was only considered in this work for comparison with previous results. This assumption leads to plane-stress effective material properties such that reduced constitutive equations are rewritten in either e-form or d-form types, respectively, as

$$\left\{\begin{array}{c} T_1 \\ T_2 \\ T_4 \\ T_5 \\ T_6 \\ \hline D_3 \end{array}\right\} = \left[\begin{array}{ccccc|c} \bar{c}_{11}^E & \bar{c}_{12}^E & 0 & 0 & 0 & -\bar{e}_{31} \\ \bar{c}_{12}^E & \bar{c}_{22}^E & 0 & 0 & 0 & -\bar{e}_{32} \\ 0 & 0 & c_{44}^E & 0 & 0 & 0 \\ 0 & 0 & 0 & c_{55}^E & 0 & 0 \\ 0 & 0 & 0 & 0 & c_{66}^E & 0 \\ \hline \bar{e}_{31} & \bar{e}_{32} & 0 & 0 & 0 & \bar{\epsilon}_{33}^S \end{array}\right] \left\{\begin{array}{c} S_1 \\ S_2 \\ S_4 \\ S_5 \\ S_6 \\ \hline E_3 \end{array}\right\}, \tag{3}$$

$$\left\{\begin{array}{c} S_1 \\ S_2 \\ S_4 \\ S_5 \\ S_6 \\ \hline D_3 \end{array}\right\} = \left[\begin{array}{ccccc|c} s_{11}^E & s_{12}^E & 0 & 0 & 0 & d_{31} \\ s_{12}^E & s_{22}^E & 0 & 0 & 0 & d_{32} \\ 0 & 0 & s_{44}^E & 0 & 0 & 0 \\ 0 & 0 & 0 & s_{55}^E & 0 & 0 \\ 0 & 0 & 0 & 0 & s_{66}^E & 0 \\ \hline d_{31} & d_{32} & 0 & 0 & 0 & \epsilon_{33}^T \end{array}\right] \left\{\begin{array}{c} T_1 \\ T_2 \\ T_4 \\ T_5 \\ T_6 \\ \hline E_3 \end{array}\right\}. \tag{4}$$

The e-form modified coefficients due to the plane stress assumption are

$$\bar{c}_{ij}^E = c_{ij}^E - c_{i3}^E c_{j3}^E / c_{33}^E \ , \ \bar{e}_{3j} = e_{3j} - e_{33} c_{j3}^E / c_{33}^E \ , \ i,j = 1,2 \ , \ \bar{\epsilon}_{33}^S = \epsilon_{33}^S + e_{33}^2 / c_{33}^E. \tag{5}$$

It can be noticed that the electromechanical coupling of major importance (in the longitudinal direction) is between the electric field and displacement in x_3 direction, E_3 and D_3, and x_1 normal stress and strain, T_1 and S_1. Therefore, it is essential to evaluate the piezoelectric e_{31}/d_{31}, elastic c_{11}^E/s_{11}^E and dielectric $\epsilon_{33}^S/\epsilon_{33}^T$ coefficients in order to qualify these materials as sensors and actuators.

3. FINITE ELEMENT HOMOGENIZATION TECHNIQUE

In order to evaluate the effective coefficients that are important to a d_{31} MFC, as discussed in the previous section, a finite element homogenization technique similar to that proposed in (Trindade and Benjeddou, 2011) is used. It consists

ISSN 2176-5480

in evaluating the average stresses, strains, electric fields and electric displacements in a Representative Volume Element (RVE) of the MFC when subjected to properly chosen mechanical and electrical boundary and periodicity conditions. Then, using the assumed constitutive equations of an equivalent piezoelectric material, as described in the previous section, it should be possible to evaluate effective elastic, piezoelectric and dielectric coefficients of the MFC. Since only a RVE of the MFC is used to perform the calculations, it is important to account for symmetric or periodic mechanical and electrical boundary conditions in directions x_1 and x_2.

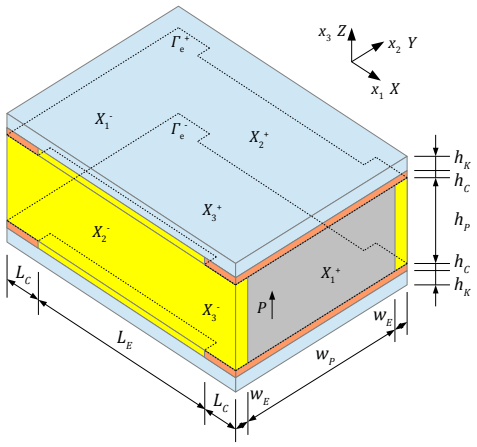

Figure 2. Representative volume element (RVE) of the d_{31} MFC.

The RVE considered in this work for the d_{31} MFC is presented in Figure 2. It is composed of a so-called 'Active Layer', with one longitudinal section of the piezoceramic macro-fibre (through-thickness poled and electroded) between two Epoxy inserts. The upper and lower surfaces of the Active Layer are then covered by one thin electrode layer each, with two Copper and one Epoxy layers representing a section of the fingered electrode layer. The electrode layers are then covered by a Kapton protective layer. The boundaries of the RVE are denoted X_1^-, X_1^+, X_2^-, X_2^+, X_3^- and X_3^+ according to Figure 2. For a more realistic analysis, additional electric potential boundary conditions are imposed at the electrodes on surfaces Γ_e^- and Γ_e^+.

Average strains and electric fields can therefore be imposed to the RVE using displacements and voltage boundary conditions, such that

$$u_i^{X_j^+} - u_i^{X_j^-} = \bar{S}_{ij}(x_j^{X_j^+} - x_j^{X_j^-}),\ i,j = 1,2,3, \tag{6}$$

$$\phi^{X_j^+} - \phi^{X_j^-} = -\bar{E}_j(x_j^{X_j^+} - x_j^{X_j^-}),\ j = 1,2, \text{ and } \phi^{\Gamma_e^+} - \phi^{\Gamma_e^-} = -\bar{E}_3(x_3^{\Gamma_e^+} - x_3^{\Gamma_e^-}). \tag{7}$$

The resulting average strains, stresses, electric fields and electric displacements in the RVE are defined as

$$\bar{S}_q = \frac{1}{V}\int_V S_q \,\mathrm{d}V,\ \bar{T}_p = \frac{1}{V}\int_V T_p \,\mathrm{d}V,\ \text{with } p,q = 1,\ldots,6, \tag{8}$$

$$\bar{E}_k = \frac{1}{V}\int_V E_k \,\mathrm{d}V,\ \bar{D}_i = \frac{1}{V}\int_V D_i \,\mathrm{d}V,\ \text{with } i,k = 1,2,3. \tag{9}$$

These integrals are approximated in Ansys$^{(\mathrm{R})}$ by a sum over averaged element values multiplied by the respective element volume divided by total volume of the RVE, such that

$$\bar{S}_q = \frac{\sum_{e=1}^N S_q^{(e)} V^{(e)}}{\sum_{e=1}^N V^{(e)}},\ \bar{T}_p = \frac{\sum_{e=1}^N T_p^{(e)} V^{(e)}}{\sum_{e=1}^N V^{(e)}},\ \text{with } p,q = 1,\ldots,6, \tag{10}$$

$$\bar{E}_k = \frac{\sum_{e=1}^N E_k^{(e)} V^{(e)}}{\sum_{e=1}^N V^{(e)}},\ \bar{D}_i = \frac{\sum_{e=1}^N D_i^{(e)} V^{(e)}}{\sum_{e=1}^N V^{(e)}},\ \text{with } i,k = 1,2,3. \tag{11}$$

where $V^{(e)}$ is the volume of the element e. $S_q^{(e)}$, $T_p^{(e)}$, $E_k^{(e)}$ and $D_i^{(e)}$ are the average strains, stresses, electric fields and electric displacements evaluated at element e. N is the total number of finite elements used to discretize the RVE.

For the evaluation of the elastic coefficients related to normal strains and stresses c_{pq}^E, $p,q = 1,2,3$, three local problems are analysed for which a normal strain S_q ($q = 1,2,3$) is applied by imposing relative normal displacements $u_q^{X_q^+} - u_q^{X_q^-}$. In order to obtain $\bar{S}_j = 0$ if $j \neq q$, the normal displacements u_j for each pair of nodes at opposing surfaces X_j^- and X_j^+

ISSN 2176-5480

are set to be equal (symmetrically coupled degrees of freedom). Then, considering the constitutive equations in (1), the effective elastic coefficients are evaluated using the following expressions

$$c^E_{pq} = \bar{T}_p/\bar{S}_q,\ p,q,= 1,2,3, \tag{12}$$

where the average stresses $\bar{T}_p$ and strains $\bar{S}_q$ are evaluated using (10).

The piezoelectric coefficients e_{31}, e_{32} and e_{33} can be also obtained from the local problems used to evaluate c^E_{1j}, c^E_{2j} and c^E_{3j}, respectively, that is where normal stress states in directions x_1, x_2 and x_3 are approximated. From the constitutive equations (1), e_{31}, e_{32} and e_{33} can be obtained by evaluating the average electric displacement D_3 such that

$$e_{31} = \bar{D}_3/\bar{S}_1,\ e_{32} = \bar{D}_3/\bar{S}_2 \text{ and } e_{33} = \bar{D}_3/\bar{S}_3. \tag{13}$$

where the average normal strains $\bar{S}_1$, $\bar{S}_2$ and $\bar{S}_3$ and electric displacement $\bar{D}_3$ are evaluated using the approximation of (10) and (11).

For the evaluation of the elastic coefficients related to shear strains and stresses c^E_{pp}, $p = 4,5,6$, other three local problems are analysed for which shear strains S_{ik} ($S_{23} = S_4/2$, $S_{13} = S_5/2$ and $S_{12} = S_6/2$) are applied to approximate a pure shear stress state in the planes $x_2 - x_3$, $x_1 - x_3$ and $x_1 - x_2$ by imposing relative shear displacements $u_i^{X_k^+} - u_i^{X_k^-}$ at surfaces X_k^+/X_k^- and $u_k^{X_i^+} - u_k^{X_i^-}$ at surfaces X_i^+/X_i^-. Moreover, the normal displacements at the boundary surfaces parallel to each shear plane of interest are symmetrically coupled to ensure zero strains perpendicular to the shear plane. Therefore, the effective elastic coefficients are evaluated in terms of the average shear stresses $\bar{T}_p$ and strains $\bar{S}_p$ using

$$c^E_{pp} = \bar{T}_p/\bar{S}_p,\ p = 4,5,6. \tag{14}$$

For both previous cases, equations (12) and (14), to ensure a short circuit electric boundary condition, the voltage degrees of freedom in the electrodes at surfaces Γ_e^- and Γ_e^+ are set to zero. Table 1 indicates symmetric boundary conditions for the electric potential along directions x_1 and x_2 for the corresponding X_1^-/X_1^+ and X_2^-/X_2^+ RVE surfaces.

For the evaluation of the blocked dielectric coefficient ϵ^S_{33}, another local problem is set up for which an electric voltage $\phi^{\Gamma_e^+} = h_P$ (in value) is applied to the electrode at surface Γ_e^+ while the voltage at the opposite electrode (at surface Γ_e^-) is set to zero so that a unitary electric field in the x_3 direction is generated. To approximate the blocked condition, the normal strains S_1, S_2 and S_3 are prevented by imposing equal normal displacements u_j ($j = 1,2,3$) for each pair of nodes at opposing surfaces X_j^- and X_j^+. The dielectric coefficient is then obtained from

$$\epsilon^S_{33} = \bar{D}_3/\bar{E}_3. \tag{15}$$

It is also worthwhile evaluating the free dielectric coefficient ϵ^T_{33}. This is done through a local problem for which an electric voltage $\phi^{\Gamma_e^+} = h_P$ (in value) is applied to the electrode at surface Γ_e^+ while the voltage at the opposite electrode (at surface Γ_e^-) is set to zero so that a unitary electric field in the x_3 direction is generated. To approximate the free condition, no mechanical displacements boundary conditions are imposed to the RVE. The dielectric coefficient is then

$$\epsilon^T_{33} = \bar{D}_3/\bar{E}_3. \tag{16}$$

Table 1 summarizes the local problems used for the characterization of the relevant material properties of the d_{31} MFC RVE. u_j^{i-} and u_j^{i+} are the displacements in direction j and ϕ^{i-} and ϕ^{i+} are the electric potentials at i-th node of opposite surfaces. q is an arbitrary non-null value.

Other coefficients of interest may be evaluated by post-processing the previous ones. The d-form piezoelectric coefficients d_{31}, d_{32} and d_{33} are approximated by inverting the three first lines of (1), such that

$$\begin{bmatrix} d_{31} \\ d_{32} \\ d_{33} \end{bmatrix} = \begin{bmatrix} c^E_{11} & c^E_{12} & c^E_{13} \\ c^E_{12} & c^E_{22} & c^E_{23} \\ c^E_{13} & c^E_{23} & c^E_{33} \end{bmatrix}^{-1} \begin{bmatrix} e_{31} \\ e_{32} \\ e_{33} \end{bmatrix}. \tag{17}$$

The effective electromechanical coupling coefficient k^2_{31} of the MFC may be evaluated as

$$k^2_{31} = \frac{d^2_{31}}{s^E_{11}\epsilon^T_{33}}. \tag{18}$$

ISSN 2176-5480

Table 1. Boundary conditions (displacement/electric potential) and relations used to evaluate the effective material properties of a d_{31} piezoelectric MFC.

Problem	X_1^-/X_1^+	X_2^-/X_2^+	X_3^-/X_3^+	Γ_e^-/Γ_e^+	Relation
1	$u_1^{i+}-u_1^{i-}=q$	$u_2^{i+}-u_2^{i-}=0$	$u_3^{i+}-u_3^{i-}=0$	-	$c_{1j}^E=\bar{T}_j/\bar{S}_1$ (12)
	$\phi^{i+}-\phi^{i-}=0$	$\phi^{i+}-\phi^{i-}=0$	-	$\phi^{i+}=0;\ \phi^{i-}=0$	$e_{31}=\bar{D}_3/\bar{S}_1$ (13)
2	$u_1^{i+}-u_1^{i-}=0$	$u_2^{i+}-u_2^{i-}=q$	$u_3^{i+}-u_3^{i-}=0$	-	$c_{2j}^E=\bar{T}_j/\bar{S}_2$ (12)
	$\phi^{i+}-\phi^{i-}=0$	$\phi^{i+}-\phi^{i-}=0$	-	$\phi^{i+}=0;\ \phi^{i-}=0$	$e_{32}=\bar{D}_3/\bar{S}_2$ (13)
3	$u_1^{i+}-u_1^{i-}=0$	$u_2^{i+}-u_2^{i-}=0$	$u_3^{i+}-u_3^{i-}=q$	-	$c_{3j}^E=\bar{T}_j/\bar{S}_3$ (12)
	$\phi^{i+}-\phi^{i-}=0$	$\phi^{i+}-\phi^{i-}=0$	-	$\phi^{i+}=0;\ \phi^{i-}=0$	$e_{33}=\bar{D}_3/\bar{S}_3$ (13)
4	$u_1^{i+}-u_1^{i-}=0$	$u_3^{i+}-u_3^{i-}=q$	$u_2^{i+}-u_2^{i-}=q$	-	$c_{44}^E=\bar{T}_4/\bar{S}_4$ (14)
	$\phi^{i+}-\phi^{i-}=0$	$\phi^{i+}-\phi^{i-}=0$	-	$\phi^{i+}=0;\ \phi^{i-}=0$	
5	$u_3^{i+}-u_3^{i-}=q$	$u_2^{i+}-u_2^{i-}=0$	$u_1^{i+}-u_1^{i-}=q$	-	$c_{55}^E=\bar{T}_5/\bar{S}_5$ (14)
	$\phi^{i+}-\phi^{i-}=0$	$\phi^{i+}-\phi^{i-}=0$	-	$\phi^{i+}=0;\ \phi^{i-}=0$	
6	$u_2^{i+}-u_2^{i-}=q$	$u_1^{i+}-u_1^{i-}=q$	$u_3^{i+}-u_3^{i-}=0$	-	$c_{66}^E=\bar{T}_6/\bar{S}_6$ (14)
	$\phi^{i+}-\phi^{i-}=0$	$\phi^{i+}-\phi^{i-}=0$	-	$\phi^{i+}=0;\ \phi^{i-}=0$	
7	$u_1^{i+}-u_1^{i-}=0$	$u_2^{i+}-u_2^{i-}=0$	$u_3^{i+}-u_3^{i-}=0$	-	
	$\phi^{i+}-\phi^{i-}=0$	$\phi^{i+}-\phi^{i-}=0$	-	$\phi^{i+}=q;\ \phi^{i-}=0$	$\epsilon_{33}^S=\bar{D}_3/\bar{E}_3$ (15)
8	-	-	-	-	
	$\phi^{i+}-\phi^{i-}=0$	$\phi^{i+}-\phi^{i-}=0$	-	$\phi^{i+}=q;\ \phi^{i-}=0$	$\epsilon_{33}^T=\bar{D}_3/\bar{E}_3$ (16)

4. COMPARISON WITH PREVIOUS RESULTS FOR MFC PROPERTIES

The finite element mesh used in Ansys$^{(R)}$ to solve the local problems and evaluate effective properties of a 5-layered d_{31} MFC RVE, using a FVF of 0.86 for the PZT+Epoxy Active Layer, is shown in Figure 3. The 3D 20-Node coupled-field solid finite element SOLID226 was used to mesh all volumes. It has the three displacement translations along the Cartesian coordinate system and the electric potential as nodal degrees of freedom.

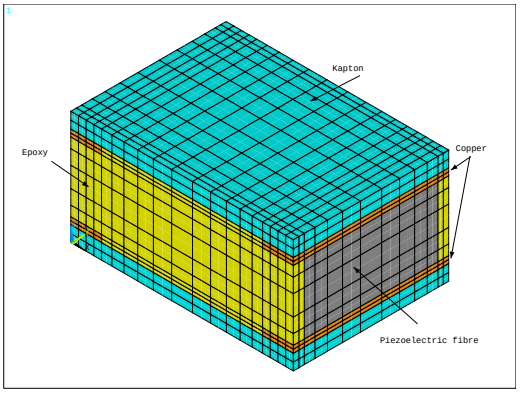

Figure 3. Finite element mesh for the full 5-layered d_{31} MFC RVE with FVF=0.86.

3211 finite elements were used considering 19 divisions in x_1 direction (11 divisions for the Epoxy layer and 4 divisions for each electrode layer), 13 divisions in x_2 direction (9 divisions for the PZT fibre and 2 divisions for the Epoxy layer) and 13 divisions in x_3 direction (5 divisions for the PZT layer, 2 divisions for each electrode layer and 2 divisions for each protective layer). The dimensions considered for this RVE (Figure 2) are $h_P = 180$ μm, $h_K = 40$ μm, and $h_C = 18$ μm, $L_E = 420$ μm, $L_C = 80$ μm, $w_E = 28.35$ μm and $w_P = 348.3$ mm (Deraemaeker et al., 2009). The material properties for the piezoceramic material Sonox P502, taken from (Deraemaeker et al., 2009), are: $s_{11}^E = s_{22}^E = 18.5$ pm^2/N, $s_{33}^E = 20.7$ pm^2/N, $s_{12}^E = -6.29$ pm^2/N, $s_{13}^E = -6.23$ pm^2/N, $s_{44}^E = s_{55}^E = 33.2$ pm^2/N, $s_{66}^E = 52.3$ pm^2/N, $d_{31} = d_{32} = -185$ pC/N, $d_{33} = 440$ pC/N, $d_{15} = d_{24} = 560$ pC/N, $\epsilon_{11}^T = \epsilon_{22}^T = 1950\epsilon_0$, $\epsilon_{33}^T = 1850\epsilon_0$. The material properties for the other constituents, taken from (Kranz, Benjeddou and Drossel, 2013), are: Epoxy – $Y = 2.5$ GPa, $\nu = 0.42$ and $\epsilon = 4.25\epsilon_0$; Kapton – $Y = 2.5$ GPa, $\nu = 0.34$ and $\epsilon = 3.4\epsilon_0$; and Copper electrode – $Y = 110$ GPa, $\nu = 0.34$ and $\epsilon = 5\epsilon_0$.

Figures 4 and 5 show the field distributions of normal stresses T_j and strains S_j ($j = 1,2$) and electric displacements D_3 resulting from the local problems #1 and #2. They were used to evaluate the plane-stress normal elastic coefficients c_{11}^E, c_{12}^E and c_{22}^E and the piezoelectric coefficients e_{31} and e_{32}.

It is noticeable from Figure 4 that, while the normal strain S_1 distribution is quite uniform, the normal stress T_1 is concentrated in the stiffer PZT fibre and Copper electrode. The electric displacement D_3 is evidently only concentrated in the PZT fibre. Within the fibre, Figure 4c shows that the electric displacement, and thus the electromechanical coupling, is more important through the mid-line and along the interface with the Epoxy material of the active layer.

As for the case of local problem #2, the normal strain S_2 is concentrated in the softer Epoxy of the active layer, while the normal stress T_2 is concentrated in the Copper electrode (Figure 5). Therefore, the Copper electrode has an important

ISSN 2176-5480

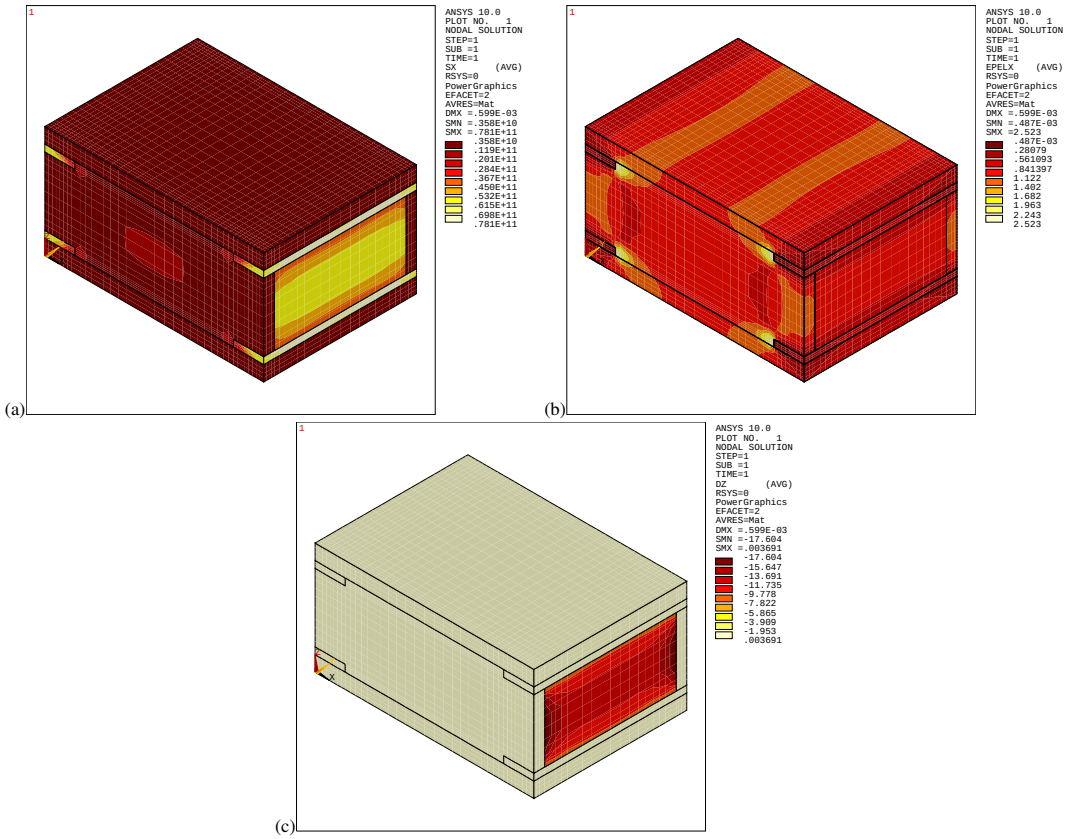

Figure 4. Normal stress T_1 (a) and strain S_1 (b) and electric displacement D_3 (c) induced by normal displacements applied to the d_{31} MFC RVE (local problem #1).

effect on the effective elastic coefficient Y_2^E. A decrease on the Copper volume fraction in the electrode layer should then lead to a decrease on the transversal (through-width) stiffness. Similarly to the previous case, the electric displacement D_3 is concentrated in the PZT fibre.

The local problems #7 and #8 are intended to evaluate the blocked and free dielectric coefficients, ϵ_{33}^S and ϵ_{33}^T, by applying a difference of electric potential on the electrodes and, hence, a uniform through-thickness electric field. Thus, the distributions of electric field E_3 and displacement D_3 are of major interest. Figures 6 and 7 present similar distributions for these two quantities, although the electric displacement values are substantially smaller for the blocked case (local problem #7, Figure 6a). The main difference between the two local problems is due to the mechanical boundary conditions. In local problem #7, the normal strain S_1 is blocked (Figure 6c) and, thus, normal stress T_1 is developed in the PZT fibre (Figure 6d). On the other hand, in local problem #8, the MFC is free to move and, thus, develop normal strains S_1 (Figure 7c) while leading to negligible normal stress T_1 (Figure 7d).

In order to validate the finite element homogenization, the evaluated effective coefficients of the d_{31} MFC were compared to previous analytical and experimental results found in the literature. Using a mixing rules technique, Deraemaeker et al. (Deraemaeker et al., 2009) evaluated effective plane-stress coefficients for the active layer of the same d_{31} MFC considered in this work. Thus, the finite element homogenization procedure presented previously was adapted to a finite element model of the active layer only by removing the electrode (Copper+Epoxy) and protective (Kapton) layers. To better compare with the results presented in (Deraemaeker et al., 2009), the Epoxy material properties provided therein were used ($Y = 2.9$ GPa, $\nu = 0.3$ and $\epsilon = 4.25\epsilon_0$) and the finite element homogenization was performed removing the boundary conditions imposing $S_3 = 0$ (in local problems 1, 2 and 7). Also, to allow comparison with the full 5-layered MFC, the electric potentials are still applied to the surfaces Γ_e^+ and Γ_e^-, shown in Figure 2. The first and second columns of Table 2 display, respectively, the results obtained by the finite element homogenization proposed in the present work and the mixing rules technique of (Deraemaeker et al., 2009). It is noticeable that the present results agree very well with the mixing rules ones. It is worthwhile to notice from Table 2 that the presence of the Epoxy filling diminishes the effective piezoelectric coefficients d_{31} and e_{31} of the active layer, compared to those of the PZT fibre alone, and also leads to an orthotropic active layer (and no longer transversally isotropic as the PZT fibre). In particular, the active layer is more effective in the longitudinal direction such that d_{31} and e_{31} are higher than d_{32} and e_{32}.

Then, the results obtained for the full 5-layered MFC with the proposed approach were compared to data provided by the manufacturer of a commercial d_{31} MFC (Smart Material Corp.) (Smart Material Co., 2009), with the same nominal

ISSN 2176-5480

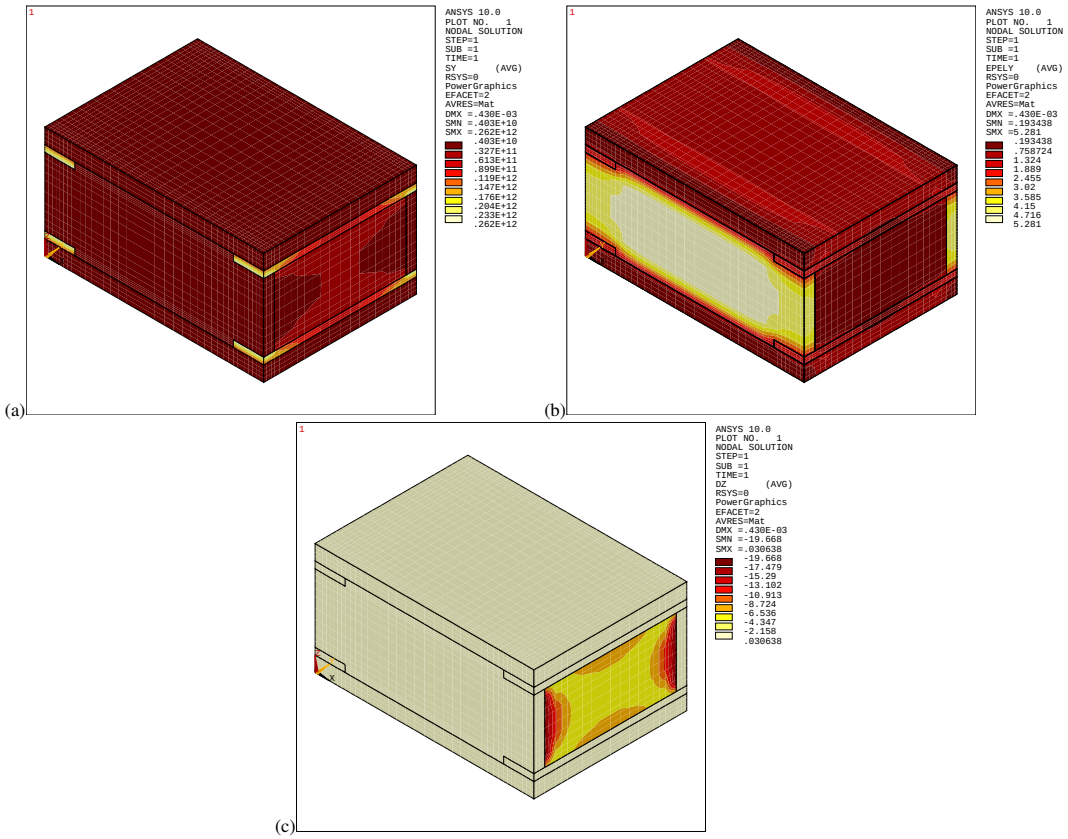

Figure 5. Normal stress T_2 (a) and strain S_2 (b) and electric displacement D_3 (c) induced by normal displacements applied to the d_{31} MFC RVE (local problem #2).

geometrical and material properties for its constituents considered in the present work. Notice that not all coefficients are provided by the manufacturer. Nevertheless, it can be concluded that the proposed approach represents very well the actual (manufactured) d_{31} MFC. The only coefficient presenting a more important error (13%) compared to the data from manufacturer is the transversal elastic modulus Y_2^E, but this may be explained by the fact that the actual width of the Copper electrode finger (L_c) is not known and was only visually approximated from a microphotography presented by the original prototype developer at NASA Langley Research Center (Wilkie et al., 2000). A wider Copper electrode finger would lead to a higher transversal elastic modulus Y_2^E. It could also affect the transversal piezoelectric coefficients e_{32} and d_{32}. The results obtained for the most important effective coefficients, Y_1^E, d_{31} and ϵ_{11}^T, are all below 4% error (3.5%, 1.3% and 0.9% respectively) compared to the data provided by the Smart Material Corp. (Smart Material Co., 2009).

Notice that the electrode and protective layers diminish substantially the effective properties of the MFC, compared to the active layer alone (see first and third columns of Table 2). In particular, the piezoelectric coefficients d_{31} and $\bar{e}_{31}$ are reduced by 6% and 33%, respectively, while the effective electromechanical coupling coefficient k_{31}^2 is reduced by 39%.

5. ANALYSIS OF THE EFFECT OF FVF AND ELECTRIC BOUNDARY CONDITIONS

In this section, the finite element homogenization technique was used to evaluate the effect of the fibre volume fraction on the main effective properties of the d_{31} MFC, namely the longitudinal Young's modulus Y_1, the piezoelectric coefficient d_{31} and the free dielectric coefficient ϵ_{33}^T. In addition, the results obtained are compared to those for the MFC Active Layer to quantify the effect of the protective and electrode layers. The results obtained for the MFC Active Layer are also compared to those obtained using a Mixture Rules technique proposed in (Deraemaeker et al., 2009).

According to (Deraemaeker et al., 2009), the effective properties of a d_{31} MFC Active Layer, composed of piezoelectric fibre (p) and Epoxy matrix (e), can be written as

$$Y_1^E = \rho Y_1^{Ep} + (1-\rho) Y_1^e \ , \ d_{31} = \rho (E_1^p / E_1) d_{31}^p \ , \ \epsilon_{33}^T = \rho \epsilon_{33}^{Tp} + (1-\rho)\epsilon_{33}^e . \tag{19}$$

where Y_1^{Ep} and Y_1^e are the longitudinal Young's moduli of the piezoelectric fibre (at constant electric field) and Epoxy matrix, respectively. ϵ_{33}^{Tp} and ϵ_{33}^e are the dielectric coefficient of the piezoelectric fibre (at constant stress) and Epoxy matrix, respectively. d_{31}^p is the piezoelectric coefficient of the piezoelectric fibre and ρ is the fibre volume fraction of the active layer.

ISSN 2176-5480

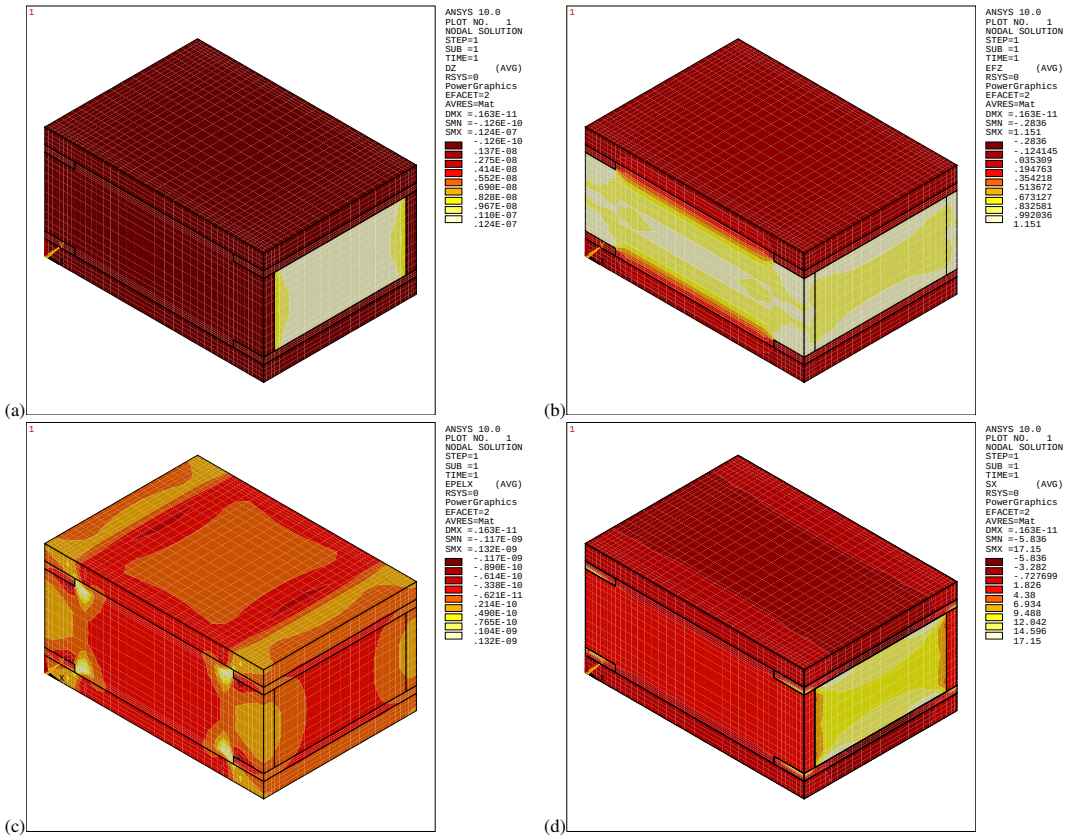

Figure 6. Electric displacement D_3 (a) and field E_3 (b) and longitudinal strain S_1 (c) and stress T_1 (d) induced by electric potential applied to the blocked d_{31} MFC RVE (local problem #7).

Table 2. Effective short-circuit material properties of d_{31} MFC and its active layer (*: values obtained post-processing data provided in the reference).

	PZT-Epoxy Active Layer		Full 5-Layered MFC	
Coefficient	Finite element	Mixing rules (Deraemaeker et al., 2009)	Finite element	Manufacturer (Smart Material Co., 2009)
Y_1^E (GPa)	46.89	47.17	31.40	30.34
Y_2^E (GPa)	17.92	16.98	19.80	15.86
Y_3^E (GPa)	–	–	9.03	–
G_{23}^E (GPa)	6.07	6.06	2.17	–
G_{13}^E (GPa)	16.91	17.00	2.42	–
G_{12}^E (GPa)	5.87	6.03	5.34	5.52
ν_{12}^E	0.39	0.39	0.36	0.31
d_{31} (pC/N)	-183.1	-183	-172.2	-170
d_{32} (pC/N)	-167.0	-153	-133.8	–
e_{31} (C/m^2)	–	–	-6.04	–
e_{32} (C/m^2)	–	–	-3.47	–
e_{33} (C/m^2)	–	–	1.48	–
$\bar{e}_{31}$ (C/m^2)	-10.35	-10.23*	-6.93	–
$\bar{e}_{32}$ (C/m^2)	-4.53	-4.05*	-4.23	–
$\epsilon_{33}^T/\epsilon_0$	1609.9	1600	1572.1	1558.6
$\epsilon_{33}^S/\epsilon_0$	1305.6	–	1179.7	–
k_{31}^2 (%)	11.0	11.2*	6.7	6.4*
k_{31}	0.33	0.33*	0.26	0.25*

It should be noted that in order to obtain (19), it is assumed that the electrodes cover the active layer entirely, which is not generally the case. Most d_{31} MFC use fingered electrodes such as the one shown in Figure 1. In this practical case, part of the Epoxy matrix is not covered by electrodes. This effect is highlighted here by performing an additional finite element homogenization of the active layer with continuous electrodes (CE) fully covering the upper and lower surfaces

ISSN 2176-5480

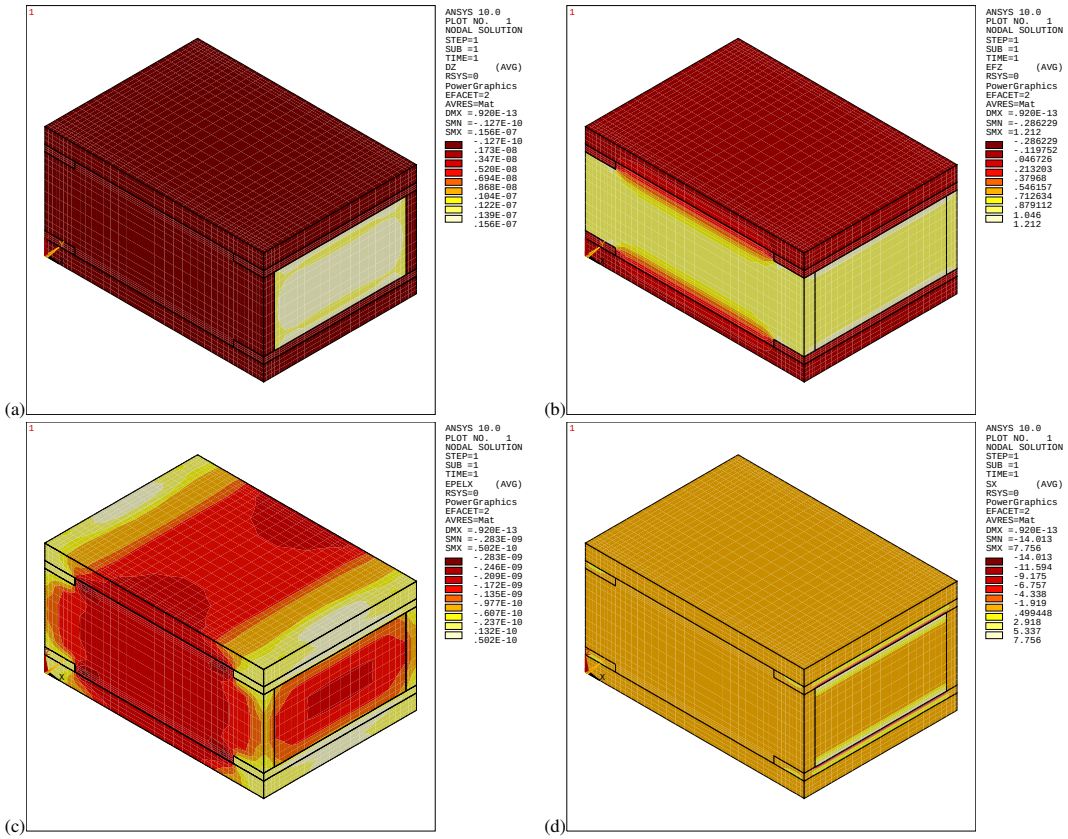

Figure 7. Electric displacement D_3 (a) and field E_3 (b) and longitudinal strain S_1 (c) and stress T_1 (d) induced by electric potential applied to the free d_{31} MFC RVE (local problem #8).

of the active layer. For that, the electric potential boundary conditions are applied to surfaces $X_3^+(x_3 = h_P)$ and $X_3^-(x_3 = 0)$ instead of surfaces Γ_e^+ and Γ_e^-.

Hence, four sets of results are presented in the following analyses, namely those obtained for the active layer only using mixture rules (MR), finite element homogenization with continuous electrodes (FE/CE) and finite element homogenization with fingered electrodes (FE), and for the full (5-layer) d_{31} MFC using finite element homogenization with fingered electrodes.

Figure 8a shows the longitudinal Young's modulus for the MFC Active Layer and for the full 5-layered d_{31} MFC. It is possible to notice that the three results for the active layer only agree satisfactorily, meaning that the electrode configuration does not affect very much the elastic behaviour of the active layer. On the other hand, the inclusion of the relatively softer protective and electrode layers leads to a significant reduction of the MFC longitudinal elastic modulus, of around 32% compared to that of the active layer. Notice that the effective longitudinal elastic modulus of the standard d_{31} MFC could be increased of around 9% by augmenting the FVF from the standard value of 86% up to 95%.

The relative dielectric coefficient $\epsilon_{33}^T/\epsilon_0$ for the MFC Active Layer and for the full 5-layered d_{31} MFC is shown in Figure 8b. In this case, it is noticeable that the electric boundary conditions do affect the results for the active layer. Indeed, the hypothesis of continuous electrodes leads to smaller dielectric coefficients, if compared to fingered electrodes (FE Active Layer), as found using both the Mixture Rules technique (MR) and finite element homogenization (FE/CE), in particular for smaller FVFs. One may also notice that the inclusion of the protective and electrode layers also leads to a reduction of the effective MFC dielectric coefficient, compared to that of the active layer (FE Active Layer). This reduction decreases with increasing FVF from 8.5%, for FVF=45%, down to 2%, for FVF=95%.

The effect of the fibre volume fraction on the piezoelectric coupling efficiency of the d_{31} MFC was also analysed. Figures 9a and 9b show its effect on the effective piezoelectric coefficient d_{31} and effective electromechanical coupling coefficient k_{31}^2, respectively.

From Figure 9a, it is possible to notice that the piezoelectric coefficient d_{31}, as the Young's modulus, is not very much affected by the electrode configuration and, thus, both finite element models (with continuous, FE/CE, and fingered, FE, electrodes) lead to similar results for the active layer. They also both agree well with the results found using the Mixture Rules technique. The inclusion of the protective and electrode layers leads to a reduction of the effective piezoelectric coefficient d_{31} that goes from 9.7%, for FVF=45%, down to 5.7%, for FVF=95%. Also, if compared with elastic modulus and dielectric coefficient, the MFC effective piezoelectric coefficient d_{31} is much less affected by the fibre volume fraction.

ISSN 2176-5480

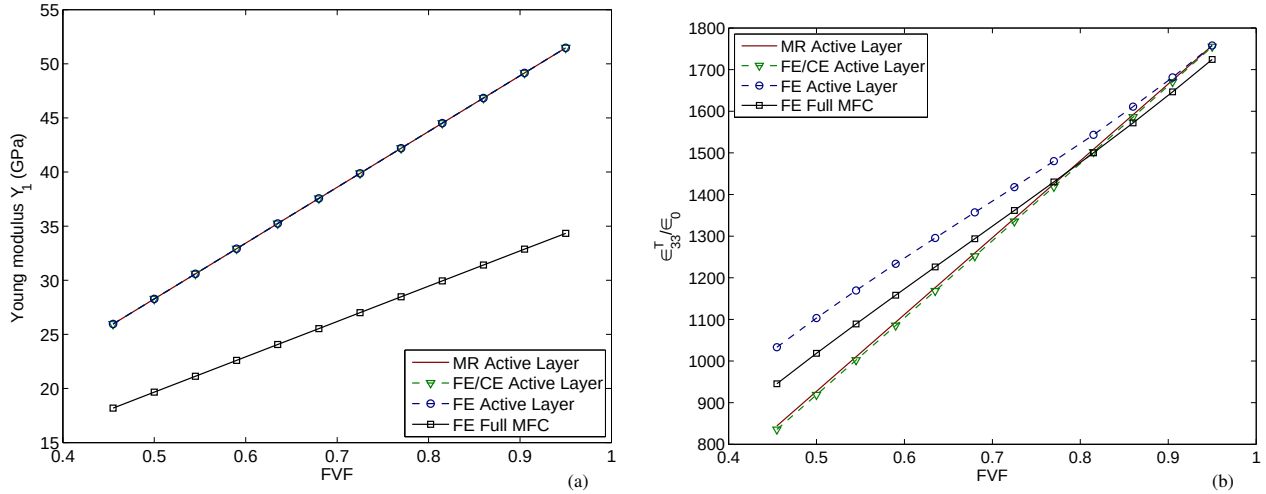

Figure 8. Young's modulus Y_1 (a) and dielectric coefficient ϵ_{33}^T (b) as function of the fibre volume fraction. Comparison between results found using mixture rules (active layer only) and finite element (active layer and full d_{31} MFC).

Hence, augmenting the FVF from 86% up to 95% yields an increase of only 1% on d_{31}.

The effect of the fibre volume fraction on the effective electromechanical coupling coefficient k_{31}^2 was also analysed and is shown in Figure 9b. The k_{31}^2 coefficient was obtained by post-processing of the results found using Mixture Rules and finite element homogenization techniques through equation (18). Due to the behaviour of the dielectric coefficient, the coupling coefficient k_{31}^2 is also affected by the electrode configuration and, thus, a continuous electrode must be considered in the finite element model (FE/CE) in order to obtain results similar to those obtained using Mixture Rules technique (MR) for the active layer. Indeed, by considering a fingered electrode configuration (FE Active Layer in Figure 9b), a significantly smaller coupling coefficient may be predicted for the active layer by the finite element homogenization, although the difference decreases substantially for increasing FVF. For FVF=86%, the coupling coefficient predicted with the fingered electrode model is 1.5% smaller than the one obtained with the continuous electrode model.

Figure 9 also shows the electromechanical coupling coefficient for the full d_{31} MFC where it is possible to notice that the inclusion of the protective and electrode layers reduce substantially, by around 39%, the effective coupling coefficient, compared to the active layer. It is also possible to observe that the k_{31}^2 coefficient is not substantially augmented by increasing the FVF from 86% ($k_{31}^2 = 6.7\%$) up to 95% ($k_{31}^2 = 6.8\%$).

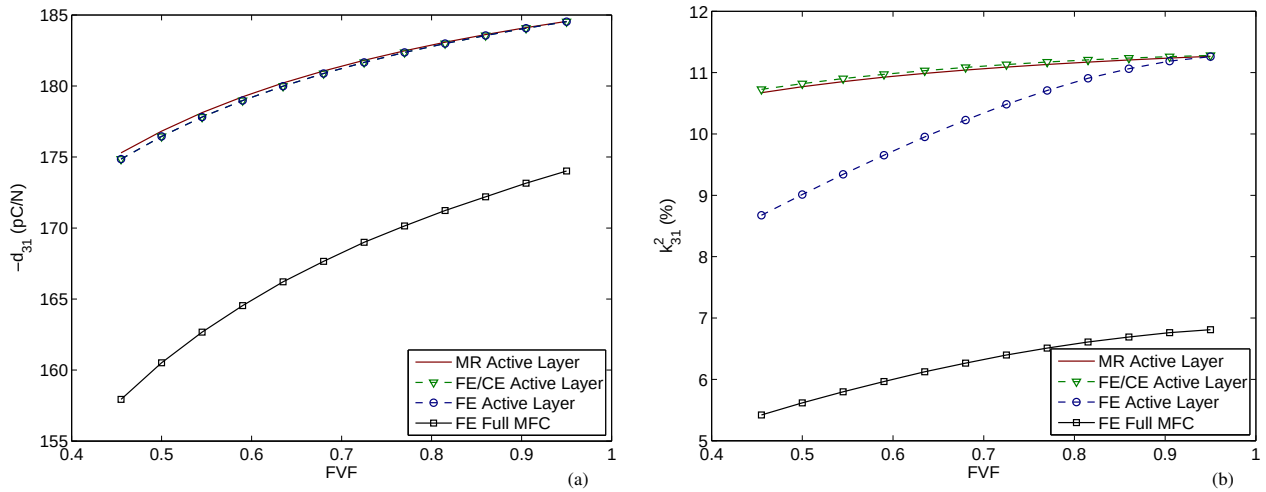

Figure 9. Piezoelectric coefficient d_{31} (a) and electromechanical coupling coefficient k_{31}^2 (b) as function of the fibre volume fraction. Comparison between results found using mixture rules (active layer only) and finite element (active layer and full d_{31} MFC).

6. CONCLUDING REMARKS

This work has presented the characterization of effective properties of a d_{31} piezoelectric MFC using a finite element homogenization technique, accounting in particular for the effect of electrode and protective layers on the effective elastic,

ISSN 2176-5480

piezoelectric and dielectric coefficients. Then, an analysis of the effect of the fibre volume fraction and electric boundary conditions on the main effective properties was presented. Results indicate that the effective properties may be substantially reduced by the protective and electrode layers and, thus, they must be accounted for in order to obtain a proper predictive model. In particular, the longitudinal elastic modulus of the d_{31} MFC may be reduced by 32% compared to the one of its active layer. The electromechanical coupling coefficient k_{31}^2 is also substantially reduced, by 39%, due to the inclusion of the protective and electrode layers.

ACKNOWLEDGEMENTS

Support of MCT/CNPq/FAPEMIG National Institute of Science and Technology on Smart Structures in Engineering, grant 574001/2008-5, is acknowledged. The second author acknowledges also the support of Comet K2 Austrian Centre of Competence in Mechatronics at Linz.

7. REFERENCES

A. Benjeddou and M. Al-Ajmi. Analytical homogenizations of piezoceramic d_{15} shear macro-fibre composites. In: Kuna, M., Ricoeur, A. (eds.) *Proceedings of the IUTAM Conference on Multiscale Modelling of Fatigue, Damage and Fracture in Smart Materials*, Freiburg (Germany), September 1-4, 2009.

A. Deraemaeker, H. Nasser, A. Benjeddou and A. Preumont. Mixing rules for the piezoelectric properties of macro fiber composites. *Journal of Intelligent Material Systems and Structures* 20(12), 1475–1482, 2009.

A. Deraemaeker and H. Nasser. Numerical evaluation of the equivalent properties of Macro Fiber Composite (MFC) transducers using periodic homogenization. *International Journal of Solids and Structures* 47, 3272–3285, 2010.

B. Gajewski. Experimental and numerical characterization of new macro-fiber-composites (MFC) for shear actuation or sensing capability. Technical Report, Fraunhofer IWU Dresden / Supmeca Paris, 2011.

W.K. Wilkie et al. Low-cost piezocomposite actuator for structural control applications. *Proceedings of SPIE International Symposium on Smart Structures and Materials* (Newport Beach), March 5-9, 2000.

B. Kranz, A. Benjeddou and W.-G. Drossel. Numerical and experimental characterizations of longitudinally polarized piezoelectric d_{15} shear macro-fiber composites. *Acta Mechanica*, to appear.

S. Raja and T. Ikeda. Concept and electro-elastic modeling of shear actuated fiber composite using micro-mechanics approach. *Journal of Intelligent Material Systems and Structures* 19, 1173–1183, 2008.

Smart Material Corp. *Macro-Fibre Composites Technical Data*, www.smart-material.com, Sarasota, 2009.

M.A. Trindade and A. Benjeddou. Finite element homogenization technique for the characterization of d_{15} shear piezoelectric macro-fibre composites. *Smart Materials and Structures* 20(7), 075012, 2011.

M.A. Trindade and A. Benjeddou. Finite element characterization and parametric analysis of the nonlinear behaviour of an actual d_{15} shear MFC. *Acta Mechanica*, to appear.

8. RESPONSIBILITY NOTICE

The authors are the only responsible for the printed material included in this paper.